136220

P.16

NASA Technical Memorandum 105947

Estimation of Unsteady Lift on a Pitching Airfoil From Wake Velocity Surveys

K.B.M.Q. Zaman and J. Panda
Lewis Research Center
Cleveland, Ohio

and

C.L. Rumsey
NASA Langley Research Center
Hampton, Virginia

Prepared for the
31st Aerospace Sciences Meeting and Exhibit
sponsored by the American Institute of Aeronautics and Astronautics
Reno, Nevada, January 11–14, 1993

NASA

ESTIMATION OF UNSTEADY LIFT ON A PITCHING AIRFOIL FROM WAKE VELOCITY SURVEYS

by

K. B. M. Q. Zaman[1] and J. Panda[2]
NASA Lewis Research Center
Cleveland, OH 44135

and

C.L. Rumsey[3]
NASA Langley Research Center
Hampton, VA 23681

Abstract

The results of a joint experimental and computational study on the flowfield over a periodically pitched NACA0012 airfoil, and the resultant lift variation, are reported in this paper. The lift variation over a cycle of oscillation, and hence the lift hysteresis loop, is estimated from the velocity distribution in the wake measured or computed for successive phases of the cycle. Experimentally, the estimated lift hysteresis loops are compared with available data from the literature as well as with limited force balance measurements. Computationally, the estimated lift variations are compared with the corresponding variation obtained from the surface pressure distribution. Four analytical formulations for the lift estimation from wake surveys are considered and relative successes of the four are discussed.

1. Introduction

As a part of a continuing research program on control of separated flows over airfoils and blades,[1,2] an experimental study of the phenomenon of dynamic stall over a periodically pitched airfoil was initiated about two years ago. The objective has been fundamental in scope: to advance the knowledge in the area, maintain in-house expertise, and aid in computational efforts. Initially, detailed phase-averaged flowfield measurements and flow visualization were carried out for specific cases of airfoil oscillation. These results have been summarized in Refs. 3 and 4.

During the analysis of the wake vorticity data, it occurred to us that the unsteady lift on the airfoil could be estimated from the vorticity flux shed into the wake. The analytical foundation and the various approximations for such estimation are deferred to a later section in the text. In short, the idea was based on estimating the change in circulation over time from the shed vorticity flux. Then by assuming a suitable convection velocity the change in the lift on the airfoil over the oscillation cycle could be estimated. The method produced lift hysteresis loops that had remarkable similarities with previous measurements.[5]

It was felt that the method deserved attention because the lift was obtained entirely from the wake survey. Determination of the forces on an oscillating airfoil is not an easy task. Force balance measurements can suffer from interference from structural resonances and static pressure distribution measurements can suffer from spatial resolution and sensor response limitations.

Subsequently, the analytical foundation of the method was studied further. Alternate formulations, such as due to Theodorsen,[6,7] and in the format of the analysis of Wu,[8] were considered. The 'noncirculatory' component of the unsteady lift, due to the inertia of the fluid moving with the oscillating airfoil, was also considered following Theodorsen's analysis. The details of these are discussed in section 2.3. Unfortunately, due to the small size of the airfoil and other experimental limitations, the lift hysteresis loops could not be measured directly for comparison for cases involving dynamic stall. Only limited results could be obtained with a force balance for a case at a very low reduced frequency (k). The comparison of the balance measurement with the estimated lift hysteresis loop, however, was quite encouraging.

It was felt during these deliberations that much insight could be gained from a computational study of the problem. One could calculate the unsteady lift from the

[1]Aerospace Engineer, Senior member AIAA
[2]NRC Research Associate, Member AIAA
[3]Aerospace Engineer, Member AIAA

computed wake velocity field similarly as done in the experiment. Computationally, however, data on actual unsteady lift variation would be available from the corresponding static pressure variation over the airfoil. Thus the validity of the estimated lift could be assessed by direct comparison. This led to a computational experiment, carried out by the third author. The computational results confirm the overall validity as well as potential deficiencies of the method under consideration. These results are described in the following.

2. Procedure and Analysis

2.1 Experimental procedure

The experiments were carried out in a low speed wind tunnel the details of which have been described elsewhere.[2] The coordinate system with respect to the airfoil are schematically shown in Fig. 1. A two-dimensional model of a NACA0012 airfoil with chord, c = 10.2 cm, and aspect ratio of 7.5, was mounted horizontally at the center (mid-height) of the test section. A pitching mechanism, described in detail in Ref. 3, was used to oscillate the airfoil about the one-quarter chord location. The oscillation amplitude and frequency could be adjusted continuously. An optical pick-up from the pitching mechanism was used to provide the reference signal for phase averaging. The experiments were conducted at chord Reynolds number, R_c = 44,000. The angle of attack was varied as $\alpha = \alpha_{mean} + \alpha_a \mathrm{Sin}(2\pi t/T)$, where T (= 1/f) is the period of oscillation.

The flowfield measurements were carried out using a crossed hot-wire probe. The probe could be traversed in the streamwise (x) direction, and up and down in y, through an automated computer controlled traversing mechanism. All measurements reported are for the x-y plane at the mid-span location. The assumption of two-dimensionality is implicit in the investigation; data on the two-dimensionality of the flowfield have been presented in Ref. 3.

As stated before, direct measurement of forces on the oscillating airfoil turned out to be difficult. Static pressure distribution measurement was not attempted due to a lack of availability of appropriate pressure transducers small enough to be fitted in the airfoil model. A force balance, using load cells,[9] was used to measure steady lift variation with α. The same balance was tried in an effort to measure the unsteady forces for the oscillating case. The problem faced was harmonic distortion; typically a harmonic near the structural resonance would become large especially at a higher oscillation frequency. For the dynamic stall case with α_{mean} = 15°, the force changes were large as the airfoil went in and out of stall and the harmonic distortion was severe even at very low values of f. With α_{mean} = 0° and smaller amplitude (α_a = 7.2°), the distortion was deemed minimal below an oscillation frequency of about 1 Hz. For this case the lift variation with α was measured and compared with the wake survey results as to be discussed in section 3.2.

2.2 Computational procedure

The computational procedure is similar to that in an earlier study conducted by the third author and reported in Ref. 2. An upwind-biased, implicit, approximate factorization algorithm which solves the thin-layer approximation to the two-dimensional Navier-Stokes equations is employed.[10] The algorithm is first-order accurate in time and second-order accurate in space. The computations are performed using a C-mesh. A quasi-one-dimensional characteristic analysis is used to explicitly determine the far-field boundary conditions on the C-part of the mesh, while extrapolation is employed at the downstream boundary. On the airfoil, no-slip, adiabatic conditions along with zero normal pressure gradient are applied. For all results presented here, the Baldwin-Lomax algebraic turbulence model is used with transition location assumed to be at the leading edge.

The unsteady motion of the airfoil is computationally simulated by oscillating the grid as a rigid body about the one-quarter chord.[11] The converged steady state solution of the flowfield at α_{mean} is used as the starting point for the unsteady calculations. The computations are performed time accurately. For estimating the unsteady lift from the wake velocity field, the velocity and vorticity data are interpolated for stationary points in the flow field at a given downstream location in the wake.

2.3 Analysis

The analytical formulations are briefly described here. For further details the reader may consult Ref. 4, in which the experimental results can also be found in detail. The unsteady lift, L(t) for an oscillating airfoil can be divided into two components; 'non-circulatory' $L_{NC}(t)$ and 'circulatory' $L_C(t)$.[7,12] The former component is due to the inertia of the fluid moved by the airfoil. This is dependent on k and can be negligible at small values of k. The 'circulatory' component is due to the vortical flow arising from the airfoil surface.

Non-circulatory part: Theodorsen provided an analysis for this component of the lift for pitching as well as plunging motion of a flat plate.[7] For pitching motion about one-quarter chord, as in the present investigation, the expression for the lift co-efficient can be written as

$$Cl_{NC}(t) = \pi \alpha_a \left(k \,\mathrm{Cos}2\pi ft - \frac{k^2}{2}\mathrm{Sin}2\pi ft\right).$$

One observes that $C\ell_{NC}$ increases as the square of k, and thus it becomes the dominant component at high values of k. It is linearly dependent on the amplitude (α_a) but independent of the mean angle (α_{mean}). Finally, $C\ell_{NC}$ at a given α is different between the upstroke and the down-

stroke, which yields a hystersis loop in its variation with α.

Circulatory part: The subject of this paper is the circulatory component which can be estimated from the vorticity flux in the wake. If one considers an impulsively started flow over a fixed airfoil, a 'starting vortex complex' is created which convects away from the airfoil. Once the steady state is reached, the net amount of vorticity shed into the wake over a finite time is zero, and there is a constant circulation around the airfoil. The latter circulation for the 'bound vortex', according to Kelvin's theorem, is equal and opposite to that of the 'starting vortex complex'. The force acting on a pair of counter-rotating vortices of circulation $+\Gamma$ and $-\Gamma$ separated by a distance x is given by,[7]

$$\text{Force} = \frac{d}{dt}(\rho \Gamma x)$$

For the steady airfoil, the 'starting vortex complex' moves away from the airfoil at the freestream velocity, so that $dx/dt = U_\infty$, and this leads to the familiar Kutta-Joukowski theorem for steady lift, $L = \rho U_\infty \Gamma$.

For the unsteady case of an oscillating airfoil, there is also a starting vortex complex, which should have a constant circulation. The circulation of the bound vortex, however, varies periodically with the oscillation. Within a finite time δt, the net amount of vorticity shed into the wake is nonzero, and again by Kelvin's theorem, this amount should be equal and opposite to the change in the circulation of the bound vortex $\delta\Gamma$ occurring within the same time δt. At any instant, the shed vorticity in the wake with circulation $-\delta\Gamma$ and the corresponding change in the bound vortex $\delta\Gamma$ can be thought of forming as a counter-rotating vortex pair which are moving away from each other at a convection velocity U_c; U_c is usually smaller than U_∞. Therefore, for the flow under consideration, the change in the lift in time δt can be estimated as

$$\delta L = \rho U_c \delta\Gamma$$

The change in the circulation $\delta\Gamma$ can be found by considering the fixed path ABCD shown in Fig. 1. For a sufficiently large path, it is reasonable to assume that all the vortical fluid is convected across the boundary CD only. For the two-dimensional, incompressible flow under consideration the time rate of change of circulation around the path ABCD is obtained, for example, from Eqn. 5.25 of Ref. 13 as

$$\frac{d\Gamma}{dt} = -\int_{CD} u\,\omega_z\,dy,$$

where ω_z ($= \partial v/\partial x - \partial u/\partial y$) is the spanwise component of vorticity. Therefore, one can write

$$\frac{dL}{dt} = -\rho U_c \int_{CD} u\,\omega_z\,dy.$$

Substituting $\xi_1(t) = \int_{CD} u\omega_z dy$ and integrating from time $t=0$ one obtains

$$L_c(t) = -\rho U_c \int_0^t \xi_1(t)\,dt + L_c(0) \qquad (1)$$

The value at the beginning of the integration $L_c(0)$, cannot be determined from the vorticity flux and is assumed to be zero. However, this is just an additive constant and the integration, carried through a period of oscillation, should provide the same shape of the lift hysteresis loop regardless of the starting point for the integration.

A caveat in Eqn. 1 is in the original formulation $\delta L = \rho U_c \delta\Gamma$. The assumption that the unsteady forces are due to the interaction of the shed vortex and the corresponding change in the bound vortex neglects, for example, the interaction of the former with the bound vortex itself as well as with the starting vortex complex. The effects due to the interactions of the shed vortex with the latter two vortex systems, however, would mostly cancel each other, and thus Eqn. 1 may be a reasonable approximation. But the validity and accuracy have remained unclear. Note also that the formulation is equivalent to the application of the Kutta-Joukowski theorem to find the differential lift from the differential circulation, albeit using the convection velocity U_c instead of U_∞ in the theorem. Of course, the convection velocity is not a clearly known quantity. It is expected to vary from case to case, e.g. when α_a and α_{mean} are changed. Thus, the choice of U_c in Eqn. 1 involves an arbitrariness.

Alternate analyses for the unsteady lift, which lead to Eqns. 2, 3 and 4, are now described. Let us emphasize here that all analyses considered have simplifications and a foolproof method is not in sight. In an attempt to assess the validity of each equation, Eqns. 1-4 will be applied to a given set of $u\omega_z(y,t)$ data. The resulting lift hysteresis loops will then be compared with available data, and with the actual lift obtained from pressure distributions in the case of the computation.

The second equation for $L_c(t)$ is based on the flutter analysis of Theodorsen.[6,7] After certain simplifications the expression for the lift co-efficient can be written in the present notations as

$$L_c(t) = -\rho U_c \int_{-10\tau}^{t} \frac{x + \frac{c}{2}}{\sqrt{(x+\frac{c}{2})^2 - (\frac{c}{2})^2}} \xi_1(t)\,dt + L_c(0), \qquad (2)$$

where ξ_1, as before, is equal to the vorticity flux $\int u\omega_z dy$ which is a function of time. As in Eqn. 1, the term $L_c(0)$

is unknown but is merely an additive constant. In order to evaluate the integral, at each time step a spatial distribution of vorticity is constructed from the temporal ω_z (y,t) data using a constant convection velocity U_c (i.e., replacing $x = -U_c t$). The integration is carried through the partial 'wavelength' from the trailing edge and then over ten additional complete 'wavelengths'. (Increasing the number of complete wavelengths beyond the first partial wavelength did not make a significant difference in the result.) Thus, one finds that the primary difference between Eqns. 1 and 2 is the weighting factor inside the integral of the latter. The weighting factor is greater than unity close to the airfoil and quickly decreases to unity for $x > c/2$. Physically, it signifies that the vortices closer to the airfoil make a larger contribution to the net lift than those which are farther away. One also notes that the weighting factor in Eqn. 2 can be expressed in a binomial series as

$$\frac{(x+\frac{c}{2})}{\sqrt{(x+\frac{c}{2})^2 - (\frac{c}{2})^2}} = (1 + \frac{1}{2}(\frac{c/2}{x + c/2})^2 - \frac{3}{4}(\frac{c/2}{x+c/2})^4 + ...).$$

Thus the leading term in Eqn. 2 becomes the same as Eqn. 1 and the difference between the two lies in the contribution from the higher order terms.

Equation 3 is adopted after Wu.[8] Starting with the Navier-Stokes equation Wu derived the expression for $L_c(t)$ as

$$L_C(t) = \rho \frac{d}{dt} \iint x \omega_z dx dy$$

This states that the force in the y direction (lift) is equal to the rate of change of the x-moment of all the vorticity in the flowfield. Note that the above equation is a generalized formulation of the relation, force = $d/dt(\rho x \Gamma)$, used to obtain Eqn. 1.

Thus, if the vorticity distribution over the entire flowfield were known the forces could be calculated accurately via the above equation. However, it would be practically impossible to measure all the vorticity, especially around the oscillating airfoil. Thus, the following approximations are needed. From the measured distribution of $\omega_z(y,t)$ at a given x, a spatial distribution is constructed by invoking the Taylor hypothesis, as was done for Eqn. 2. The unsteady lift, acting at mid-chord, is then approximated as

$$L_c(t) = -\rho \frac{d}{dt} \int_{-10T}^{t} (x+\frac{c}{2}) \xi_1(t) dt + L_c(0). \quad (3)$$

The fourth equation follows from the fact that the circulation around the airfoil at any instant is equal to the line integration of the velocity around the path ABCD (Fig. 1). For a large boundary ABCD this can be approximated as, $\Gamma(t) = \int_{CD} \langle v \rangle (t)\, dy$. Therefore, as done for Eqn. 1, one can write,

$$L_c(t) = -\rho U_c \int_{CD} \langle v \rangle (t) dy \quad (4)$$

Note that if $\langle v \rangle (t)$ represents the total phase averaged transverse velocity (including the long time average), the instantaneous total lift is evaluated by Eqn. 4.

Method of calculation: In the experiment, phase averaged axial velocities $\langle u \rangle$, $\langle v \rangle$ and the spanwise component of vorticity $\langle \omega_z \rangle$ are used to evaluate all of the above equations. In the computation, the instantaneous values of these quantities are used. The full expression for the periodic variation of the lift coefficient $C\ell_c$ is approximated, say from Eqn. 1, as

$$Cl_c(t) = -2\frac{U_c T}{c} \int_0^{t^*} \int_{CD} \langle u \rangle^* \langle \omega_z \rangle^* dy^* dt^*.$$

The superscript, *, represents non-dimensionalized quantities (lift is nondimensionalized by $\frac{1}{2}\rho U_\infty^2 c$, $\langle \omega_z \rangle$ by U_∞/c, y by c and t by T). From the actual discrete measurements of $\langle \omega_z \rangle^*_{ij}$ and $\langle u \rangle^*_{ij}$ the above equation at any time step $n+1$, $1 \le n \le NT$, is evaluated as follows

$$Cl_c(n+1) = -2\frac{U_c T}{c} \sum_{i=1}^{n} \sum_{j=1}^{NY} \langle u \rangle^*_{ij} \langle \omega_z \rangle^*_{ij} \Delta y_j^* \Delta t_i^*.$$

As stated before, $C\ell_c(1)$ is assumed to be zero.

As discussed in Ref. 4, the measurements in the immediate vicinity of the airfoil trailing edge are marked by hot wire errors due to large flow angularity and occasional flow reversal. Thus all $\omega_z(y,t)$ measurements are carried out at a downstream location, typically at $x_{meas}/c = 0.3$. This, however, introduces a time lag between the instants of measurement and the corresponding 'events' taking place over the airfoil. This time lag is estimated as, $-x_{meas}/U_c$, and accounted for in the calculation of the lift variation.

An interesting condition arising from the requirement of finite lift on the airfoil is that the total change of lift over one complete period of oscillation should be zero. Therefore, the above calculation requires

$$\sum_{i=1}^{NT} \sum_{j=1}^{NY} \langle u \rangle^*_{ij} \langle \omega_z \rangle^*_{ij} \Delta y_j^* \Delta t_i^* = 0.$$

Usually, due to measurement or computational errors this condition is not satisfied. This leads to $C\ell_c(1) \neq C\ell_c(NT+1)$, i.e., an unclosed hysteresis loop. For

brevity, the deviation of this sum from zero is distributed over the entire cycle and only the resulting closed loops are presented. The 'closing error' expressed as,

$$\%\text{error} = \frac{\sum_{i=1}^{NT}\sum_{j=1}^{NY} \langle u\rangle^*_{ij}\langle\omega_z\rangle^*_{ij}\Delta y^*_j\Delta t^*_i}{\sum_{i=1}^{NT}\sum_{j=1}^{NY} |\langle u\rangle^*_{ij}\langle\omega_z\rangle^*_{ij}|\Delta y^*_j\Delta t^*_i} \times 100,$$

is listed in table 1 for a few cases considered in this paper. The denominator in the above expression represents the sum of the absolute values of all vorticity shed in a cycle. This is referred to as the 'absolute vorticity flux' which, in the experiments, was found to be approximately a constant for a given value of α_{mean} and independent of k. The reader is referred to Ref. 4 for further discussion of these aspects.

3. Experimental results

Figure 2 shows a sequence of smoke-wire flow visualization photographs for a case involving dynamic stall, at various phases of the cycle. Frames (a) to (f) show phases when the angle of attack (α) is increasing (upstroke) and frames (g) to (j) show phases when α is decreasing (downstroke). As α increases, a clockwise vortex forms on the airfoil surface (frame d). This is the "dynamic stall vortex" as referred to by previous researchers. With further increase in α, the DSV moves towards the trailing edge. When it reaches the trailing edge, a counter-clockwise vortex starts to form near the trailing edge (frame f). The counter-clockwise vortex, referred to as the trailing edge vortex (TEV), grows quickly underneath the DSV (frames f and g) and lifts the latter from the airfoil upper surface. The DSV and the TEV combine to form a structure whose cross section looks like a mushroom. The 'mushroom' structure evolves, moves upward and increases in size as it convects downstream (Frames h, i and j). In frame (i), at about 2½ chords from the trailing edge, its transverse extent is already very large and measures about 3 chords. After the passage of the 'mushroom' structure, frames (j) and (a) indicate the passage of a few smaller vortices before the cycle is repeated.

While the DSV has been discussed in many previous papers on dynamic stall, the TEV and the 'mushroom' structure have remained relatively unnoticed. Such structures were observed by only a few.[14,15] The intense TEV and the enormous 'mushroom' structure could be quite significant in blade vortex interaction and aerodynamic noise generation, especially in configurations involving rows of blades. A computational study, using a multiple-scale turbulence model, was carried out recently for the conditions of Fig. 2 involving the dynamic stall.[16] Despite some differences with the experiment, the computation also yielded a similar sequence of events involving the DSV and the TEV.

Detailed phase averaged flow field measurements were carried out for the flow condition of Fig. 2, and reported in Ref. 3. An example of the sets of data that led to the unsteady lift estimation is shown in Fig. 3(a). The temporal distribution of the phase averaged azimuthal component of vorticity, measured at x/c = 0.3, and over a complete cycle is shown in this figure. The axial and transverse velocity components, ensemble averaged typically over 80 cycles, were measured at three closely spaced x-stations with x/c = 0.3 being the middle one. Central differencing provided $\partial\langle v\rangle/\partial x(y,t)$ while the term $\partial\langle u\rangle/\partial y(y,t)$ was evaluated by least squares fitting of the $\langle u\rangle(y,t)$ profiles. These two terms provided the spanwise vorticity which was non-dimensionalized as, $\langle\omega_z\rangle^* = \langle\omega_z\rangle c/U_\infty$.

While the pictures in Fig. 2 were obtained at an earlier date for k = 0.2, the somewhat lower k (=0.16) in Fig. 3(a) was chosen for use in evaluating Eqns. 1-4 so that the estimated unsteady lift could be compared with available data from the literature. However, the sequence of events in the flow at these two values of k are very similar. A scrutiny of the data of Fig. 3(a) identifies the DSV and the TEV as the concentrated lumps of positive and negative vorticity around t/T = 0.5 (α = 25°). (The sequence of events marked I, II, III and IV will be described later.) The vortical structures appear compressed in the temporal distribution because a full wavelength is captured in Fig. 3a while only a fraction of the wavelength is represented in the pictures of Fig. 2. The successive lumps of vorticity in Fig. 3(a), on the right of the TEV, represent a few additional vortices shed after the passage of the DSV-TEV pair.

Figure 3(b) shows similar $\omega_z(y,t)$ data for α_{mean} = 0° and α_a = 7.2°, a case for which force balance measurements could be performed so that the lift variation estimated from the vorticity data could be compared directly. One observes that because of the small α_{mean} and α_a the vorticity distribution in this case is devoid of large concentrations and shows only a mild undulation.

3.1 Lift variation estimated for the dynamic stall case

The circulatory component of the lift coefficient, corresponding to the data set of Fig. 3(a), is shown in Figs. 4(a)-(d) as obtained by Eqns. 1-4, respectively. The data are shown as a function of α for a complete cycle. One finds that the estimates from Eqns. 1-3 are by and large comparable and differences occur mainly where there are steep variations. For example, the magnitude of the large drop in the lift around 25° is predicted differently by the three equations. Since Eqn. 3 involves differentiation, the resulting curve appears somewhat 'jagged'. The extent of the lift hysteresis loop, however, appears to be significantly 'underpredicted' by Eqn. 4. Unfortunately, the relative accuracy of the four predic-

tions could not be judged directly as force balance measurement was not possible for this case (section 2.1).

The circulatory component of $C\ell$ from Fig. 4(a) is added to the corresponding non-circulatory component (section 2.3) and the sum is shown in Fig. 5(a). The noncirculatory component is shown as the superimposed dashed curve. Since it is derived for inviscid flow about a flat plate the non-circulatory component should be regarded as an approximation. However, it is small and the total unsteady $C\ell$ of Fig. 5(a) can now be compared with data from the literature. (As discussed before, the data in Fig. 5(a) only show departure from the steady lift, which is an unknown constant. In this figure the $C\ell$ values are referenced to the value at $\alpha = 5°$ where it is assumed to be zero). The data of McAlister et al.,[5] obtained by static pressure distribution measurement at about the same value of k, are shown in Fig. 5(b). The overall features of the $C\ell$ variation in Fig. 5(a) can be seen to be similar to the data set of Fig. 5(b). The slope of the upper branch (between I and II) and the small anti-clockwise loop around $\alpha = 25°$ (between III and IV) in Fig. 5(a) are in reasonable agreement with the data of Fig. 5(b). The main difference occurs in the lower branch of the loop. But some differences are expected as the lift hysteresis loop is known to be sensitive to other flow parameters besides k. The Reynolds number R_c was quite different between the two experiments ($4.4x10^4$ in the present case as opposed to $4.8x10^5$ in Ref. 5). The undulations on the lower branch, however, have been observed in other experiments.[17] Before continuing to evaluate the unsteady lift estimation technique, let us briefly discuss the observed variations in the lift in Fig. 5(a).

Lift hystersis loop vis-a-vis measured vorticity: Obtaining the lift hysteresis loop from the vorticity data provided a unique opportunity to relate its various features with the vortical structures observed through the vorticity maps and the flow visualization. The variations in the lower branch of the lift hysteresis loop, as discussed in the foregoing, are believed to be real and due to the passage of the successive vortices following the DSV. As discussed earlier, for the case under consideration, nearly all the positive (clockwise) vorticity generated from the airfoil suction surface accumulates to form the DSV during the upstroke (between points I and II in Figs. 3a and 5a). This is reflected in the wake as a depletion of positive vorticity. But the negative vorticity generated from the pressure surface is shed in the wake as usual. Qualitatively, a large negative vorticity in the wake is equivalent to a 'starting vortex' and a large positive vorticity is equivalent to a 'stopping vortex'. When the former is shed, circulation around the airfoil as well as lift increases, while shedding of the latter causes a drop in the lift. Thus, between points I and II the airfoil lift increases and between points II and III, when the DSV containing positive vorticity is shed, the lift drops. The rebounding of the lift near the highest angle of attack during the downstroke (III to IV) is due to the shedding of the TEV which contains a concentration of negative vorticity. The undulations in the lower branch of the hysteresis loop occur due to the passage of a few more, relatively weaker positive and negative vortices following the DSV and the TEV (IV to I).

3.2 Lift variation for $\alpha = 0° + 7.2°Sin2\pi ft$

The temporal distribution of vorticity for this case, at k = 0.028 (f = 0.57 Hz) and R_c = 44,000, was shown in Fig. 3(b). The corresponding unsteady lift variation was measured with a force balance and also estimated using the above mentioned calculation procedures. The very low value of k was chosen to minimize harmonic distortions of the load cell signal (section 2.1). The force balance data are presented first followed by a comparative evaluation of the calculations.

Force balance data: The unsteady lift variation measured by the force balance is shown in Fig. 6. The steady state lift variation, also measured by the same force balance is shown by the dashed line. The latter shows a kink around $\alpha = 0°$, which, as discussed in the following, is believed to be due to laminar separation at this low operating Reynolds number. Such departure from linear variation due to laminar separation has been observed by others (e.g., Ref. 18).

The unsteady measurements show a hysteresis loop even at this low oscillation frequency. The variation in the upper and the lower branches of the loop bear similarities with the steady state lift variation. At first sight, the hystersis loop is unexpected, since the dynamic stall phenomenon should not appear when the airfoil is oscillated within its static stall limit.[19] However, it is believed that laminar separation is responsible for the hystersis loop in much the same way as for the kink in the steady lift variation. For the steady airfoil, the flow remains separated on both surfaces around $\alpha = 0°$ resulting in near zero lift.[18,9] Only when the angle of attack is increased (or decreased) sufficiently, does the flow reattach on the upper (or lower) surface resulting in the increase (or decrease) in lift. For the case of oscillation, the extent of the laminar separation on a given surface of the airfoil presumably depends on the direction of motion. In other words, the extent of the separation at a given value of α on a given surface of the airfoil during upstroke is different from that occurring during downstroke. This apparently causes the observed hystersis loop in the $C\ell$ curve.

Estimated lift variation: Figures 7(a)-(d) show the lift hysteresis loops constructed from the data of Fig. 3(b) using Eqns. 1-4, respectively. The solid line represents the calculated circulatory part and in each figure this is plotted such that the mean $C\ell$ at $\alpha = 0°$ matches the

corresponding steady state value of the $C\ell$. The steady state lift variation measured by the force balance is shown as the dashed line. The non-circulatory component is negligible at this low value of k. Again, the lift hysteresis loops obtained by Eqns. 1-3 are found to be essentially similar and differences occur in the details. These loops are also very similar to the actual $C\ell$ variation of Fig. 6 and the maximum and minimum amplitudes are well represented. The lift curve obtained by Eqn. 4, however, is clearly different. It is not completely clear but it appears that a limited transverse distance in the integration is responsible for this underprediction. The computational results in the next section seem to confirm this. It should be emphasized here that the data of Fig. 7 were very sensitive to small changes, especially in oscillation frequency and in hot-wire calibration. The vorticity flux was small and thus accurate measurement was difficult; every time these data were retaken there was some difference in the lift hystersis loop.

The experimental results for the small amplitude low k case provided the confidence that the unsteady lift measurement technique under consideration can yield results that are reasonably in agreement with the actual lift variation. Computational results presented in the next section add further credence to the technique.

4. Computational results

The computations were carried out for the NACA-0012 airfoil at R_c=44,000. In order to obtain more cycles of oscillation for a given number of iterations and other limitations a value of k=0.3 and a freestream Mach number (M) of 0.3 were chosen for these computations. Furthermore, in order to avoid separated flows, for which the application of the Baldwin-Lomax turbulence model is questionable, a small amplitude oscillation condition of $\alpha = 2° + 2°\sin 2\pi ft$ was chosen. The nonzero α_{mean} was chosen so that numerical errors would show up in the cumulative vorticity flux used to compute the unsteady lift. (A symmetric condition with α_{mean}=0 produced cancellation of errors with a resultant 'closing error' equal to zero). Note that at the chosen R_c, laminar separation would be expected in the experiment even at these low values of α_{mean} and α_a. But this is not the case in the computation as boundary layer transition is assumed from the leading edge. As stated before, the idea here was to compute the lift variations using Eqns. 1-4 and compare those with the exact lift variation obtained from the static pressure (C_p) distribution, so that the validity of the four equations could be assessed.

First, the adequacy of computational mesh density and domain extent were tested. Figure 8(a) shows the lift co-efficient variation with time, obtained from the C_p-distribution, for three mesh densities. Time in this and the following figures is nondimensionalized by the chord and the speed of sound, and referenced to the instant when the unsteady calculations are initiated. These results show little variation, particularly on the two finer grids, indicating grid-convergent results for the lift history. Thus, the middle mesh density of 193x73 was deemed sufficient for the computations. Similarly, Fig. 8(b) demonstrates little difference in the results for computational domains extending more than 8 chords from the airfoil. Most of the later computations are performed with the domain having 14c extent. Although not shown the lift coefficient variation with time obtained by Eqns. 1-4 also exhibits convergent results for the aforementioned grid density and domain. The effect of time step on the C_p-determined lift history was also investigated. Three different time steps were tried, for a total of 349, 698 and 1396 steps (iterations) per cycle. All results were nearly identical to those shown in Fig. 8. Hence, 698 steps per cycle were deemed to be sufficient.

The lift variation obtained from the Cp-distribution (Fig. 8) is shown as a function of α in Fig. 9 for a complete cycle. The corresponding non-circulatory component calculated from the equation given in section 2.3 is shown by the dashed line in Fig. 9. The lift variation goes through hysteresis even for these small values of α_{mean} and α_a. The hysteresis is mainly due to the non-circulatory component occurring at the relatively high k. It is also apparent that the calculated non-circulatory component does not fully account for the observed extent of the hysteresis loop. The discrepancy is believed to be due to simplifying assumptions in the equation for the non-circulatory component. For example, the airfoil thickness and the effect of the boundary layer are not taken into account in the formulation.

While the lift variation obtained from C_p-distribution, e.g., in Fig. 8, is "exact", the predictions from Eqns. 1-4 involve a phase lag depending on the measurement station. If such a phase lag is not accounted for properly it would drastically alter the shape of the lift hysteresis loop. For simplicity, however, the rest of the computational results are presented as a function of time only. Fig. 9 serves to provide an idea how these time variations would convert into the hysteresis loops.

The $C\ell$ variations obtained by Eqn. 1, with data from different x-stations, are compared in Fig. 10 with the actual $C\ell$ variation. Note that the results of Eqn. 1 represent the unsteady components, and for easy comparison these are plotted such that the average of each matches the average of the actual lift variation. The results of Eqn. 1 are shown without any correction for the phase lag. Recall that in constructing the hysteresis loops from the experimental data (section 3.1) such a correction was done. The data were referenced to the trailing edge of the airfoil assuming a convection velocity U_c. As expected, Fig. 10 shows a progressive phase lag with increasing distance of the measurement station. The phase lag, of course, arises due to the fact that there is a finite time required for the 'events' occurring over the

airfoil to convect down to the measurement station. Nevertheless, it is amply clear from Fig. 10 that the amplitudes of the lift variation are reproduced very well by Eqn. 1.

The times at which the peak in the $C\ell$ occurred at different x (Fig. 10) are shown in Fig. 11. A straight line can be reasonably fitted through the data. This indicates that it is reasonable to assume a constant convection velocity, in conjunction with the equations, over the x-range covered. The slope of the straight line, however, yields a value of U_c approximately equal to the freestream velocity (U_∞). Note that for the data presented in section 3, based on experimental estimates, $U_c=0.6U_\infty$ and $U_c=0.6U_\infty$ were used for the $15°\pm10°$ and the $0°\pm7.2°$ cases, respectively. As stated before, it is not unexpected that U_c varies from case to case, and this represents one of the arbitrary aspects in the method under consideration. However, $U_c = U_\infty$ is clearly appropriate for the case chosen in the computation, and this is what has been used for the rest of the computational results.

The extrapolation of the straight line in Fig. 11 also shows that when accounting for the phase lag the data should be referenced to a location approximately 0.3c from the leading edge (x/c = -0.7). (The horizontal line represents the time when the C_p-determined lift has the peak.) In other words, only when the data are shifted by a time, $\delta t = (x+0.7c)/U_c$, would the comparison with the actual $C\ell$ variation be appropriate. It is not clear if this reference location would be the same for the dynamic stall case. However, if that were the case, the hysteresis loops constructed from the experiment would appear slightly different as in those cases the phase lag was corrected by referencing the data to the trailing edge.

Figure 12(a) shows the $C\ell$-variation obtained with Eqn. 1 for three different sampling rates as indicated. The results indicate that 50 samples/cycle is adequate for resolving the lift variation. This rate was used for the experimental data and is also used for the rest of the computational data.

Since a grid system moving with the airfoil was used for the computations, the data had to be interpolated for stationary points in the wake at a given downstream station in order to emulate the experimental procedure. Fig. 12(b) shows lift variations obtained with Eqn. 1 for the indicated number of integration points. A given number of integration points are spaced in the y-direction at a given x. The distance between the points is variable; it is the smallest at y = 0 and increases geometrically with distance. Clearly, for the transverse extent chosen (14c), 22 intgration points misses the vortical region in the wake and results in near zero lift amplitudes. As the spatial resolution is improved from 194 points (corresponding to a minimum spacing of 0.01c) to 300 points (minimum spacing of 0.001c), convergence in the result is achieved. The 300 point integration is performed for the rest of the results.

It should be mentioned here that the exercises done in Figs. 9 through 12 were repeated with the other three equations and the same inferences were made. The predictions of Eqns. 1-4 from the same set of data, at x/c = 0.5, are compared in Fig. 13. The transverse extent over which the integration was performed was varied for each case. For Eqns. 1-3 changes of the transverse extent did not make a difference in the predicted lift variation. Clearly, Eqns. 1 and 2 did well in predicting the lift variation. As in the experimental results, Eqn. 3, due to the differentiation involved, yielded a somewhat 'jagged' lift variation. For small transverse extent in the integration, Eqn. 4, as in the experimental results, underpredicted the amplitudes. (The transverse extent in the experiment was approximately 1.5c). However, when the integration distance is sufficiently large (> 16c), clearly Eqn. 4 also does just as well as Eqns. 1 and 2 in the prediction.

Thus, the computational results for the chosen flow confirm that the wake survey method may be a viable approach for determination of unsteady lift on an airfoil.

5. Concluding remarks

A method of estimating the unsteady component of lift from wake velocity surveys is considered in this paper. The analytical foundations are discussed and four alternate equations with different approximations are considered. It is found that the lift hysteresis loops estimated with most of these equations compare well with limited force balance data as well as with data from the literature. The method is a novel one and could be of interest in similar experiments in the future as the lift hysteresis loop is obtained strictly from wake surveys without direct force or static pressure distribution measurements.

The computational experiment carried out for a specific low amplitude case of airfoil oscillation supports the inferences made from the experimental data. These results confirm that the amplitudes of lift variation obtained by most of the equations are well in agreement with the actual lift variation. The latter is obtained from the Cp-distribution over the airfoil. These results also reaffirm that the convection velocity to be used in the method can vary from case to case. Even though a change in the convection velocity represents a change in a multiplicative constant for the result, its choice represents a main arbitrariness in the method. The computational results showed that in order to account for the phase lag in the estimated lift variation, the data obtained at a certain downstream station should be referenced to a location approximately 0.3 chords from the leading edge.

Of the four considered, Eqns. 1 and 2 are found to be equally successful in predicting the unsteady lift. Since Eqn. 1 is relatively simple and has the similarity

with the theorem for calculating steady lift from the circulation, this would be our recommendation. With this equation the 'circulatory' component of the lift is estimated as L_c = density x U_c x cumulative vorticity flux shed by the airfoil from the beginning of an oscillation period, where U_c is an appropriate constant convection velocity. From the computational results, it appears that this equation is relatively insensitive to sampling rate and integration extent, but a sufficient number of integration points are necessary to obtain accurate results. Equation 4 should also be considered attractive, as it requires the simplest of measurements involving only one component of velocity in the wake. However, the transverse extent over which this measurement needs to be done in order to obtain convergent results is large. Equation 4, thus, may not be suitable for most wind tunnel experiments.

REFERENCES

[1]Rice, E. J. and Zaman, K. Control of shear flows by artificial excitation, *AIAA paper no. 87-2722*, 1987.

[2]Zaman, K. B. M. Q., McKinzie, D. J. and Rumsey, C. L. A natural low-frequency oscillation of the flow over an airfoil near stalling condition. *J. Fluid Mech.* **202**, 403-442, 1989.

[3]Panda, J. and Zaman, K.B.M.Q. Experimental investigation of the flowfield of an oscillating airfoil. *AIAA Paper 92-2622*, 1992.

[4]Panda, J. and Zaman, K.B.M.Q. Experimental investigation of the flowfield of an oscillating airfoil and estimation of lift from wake surveys. *J. Fluid Mech.*, 1992 (submitted).

[5]McAlister, K.W., Pucci, S.L., McCroskey, W.L. and Carr, L.W., An experimental study of dynamic stall in advanced airfoil sections, vol. 2, pressure and force data, *NASA TM 84245*, 1982.

[6]Theodorsen, T. General theory of aerodynamic instability and the mechanism of flutter. *NACA report 496*, 1935.

[7]Bisplinghoff, R.L., Ashley, H. and Halfman, R.L., *Aeroelasticity*, Addison-Wesley, 1955.

[8]Wu, J. C. Theory of aerodynamic force and moments in viscous flows. *AIAA J.* **19**, no. 14, 432-441, 1981.

[9]Zaman, K. B. M. Q. and McKinzie, D. J. Control of laminar separation over airfoils by acoustic excitation. *AIAA J.* **26**, no. 7, 1075-1083, 1991.

[10]Rumsey, C.L., Thomas, J.L., Warren, G.P. and Liu, G.C., Upwind Navier-Stokes solutions for separated periodic flows, *AIAA J.*, vol. 25(4), pp. 535-541, 1987.

[11]Rumsey, C.L. and Anderson, W.K., Parametric study of grid size, time step, and turbulence modeling on Navier-Stokes computations over airfoils, *AGARD-CP-437*, vol. 1, 1988.

[12]Batchelor, G. K. *An introduction to fluid dynamics*. Cambridge Univ. Press, 1967.

[13]Potter, M. C. and Foss, J. F. *Fluid Mechanics*. Great Lakes Press, Inc, 1982.

[14]Robinson, M. C., Helin, H. E. and Luttges, M. W. Control of wake structure behind an airfoil. *AIAA paper 86-2282*, 1986.

[15]Gad-el-Hak, M. and Ho, C-M. Unsteady vortical flow around three-dimensional lifting surfaces. *AIAA J.* **24**, no. 5, 713-721, 1986.

[16]Kim, S.-W., Zaman, K.B.M.Q. and Panda, J., "Calculation of unsteady transitional flow over an oscillating airfoil", *ASME Fluids Engineering summer Meeting*, Washington, D.C., June 20-24, 1993 (to be presented).

[17]Leishman, J.G. 1990 Dynamic stall experiments on the NACA 23012 aerofoil. *Experiments in Fluids*, **9**, 49-58.

[18]Muller, T. J. and Batill, S.M. Experimental studies of separation of a two-dimensional airfoil at low Reynolds numbers. *AIAA J.* **20**, 475-463, 1982.

[19]Carr, L. W. Dynamic stall - Progress in analysis and prediction. *AIAA Paper no. 85-1769-CP*, AIAA Atmospheric Flight Mechanics Conference, 1985.

Table 1. 'Closing error' for a few cases.

Method	α	k	%closing error
Computation x/c = 0.5	2°± 2°	.3	-0.71
Computation x/c = 1.5	2°± 2°	.3	-0.86
Experiment	15°± 10°	.16	4.04
Experiment	0°± 7.2°	.028	1.6

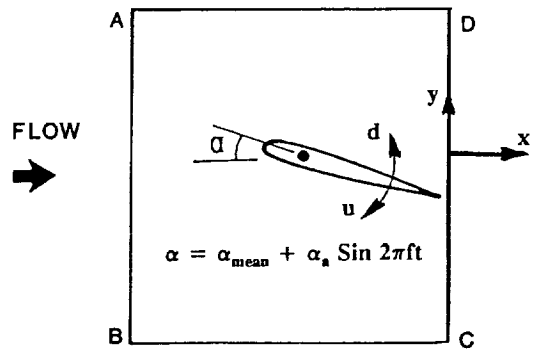

Fig. 1 Schematic of airfoil, co-ordinate system, and control volume for calculation of unsteady circulation; "u" and "d" denote increasing α (upstroke) and decreasing α (downstroke).

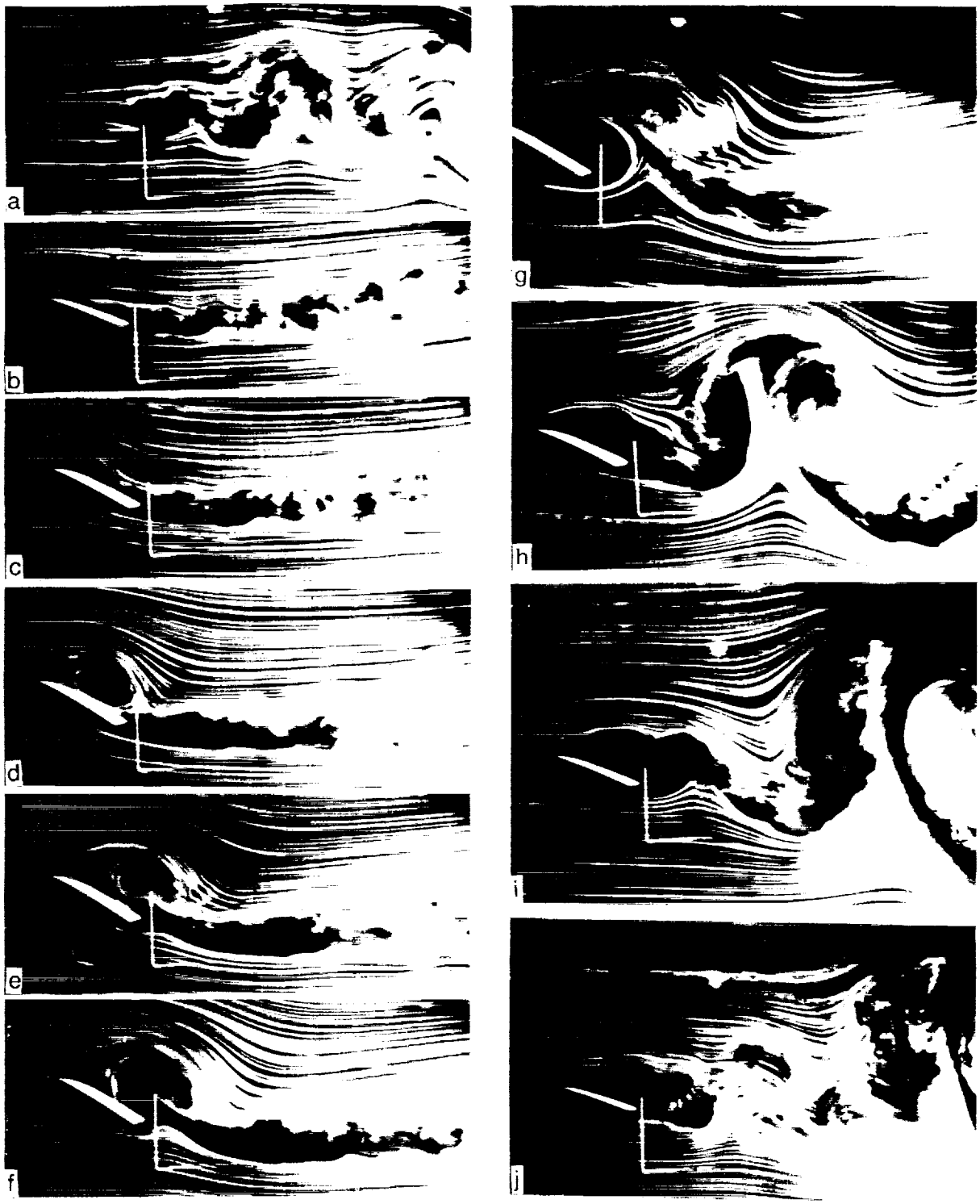

Fig. 2 Smoke-wire flow visualization photographs at different phases of oscillation cycle; k = 0.2, α = 15° + 10°sin2πft. Approximate α for pictures a to j are 5°u, 14°u, 20°u, 22°u, 24°u, 25°u, 25°d, 20°d, 16°d, 12°d.

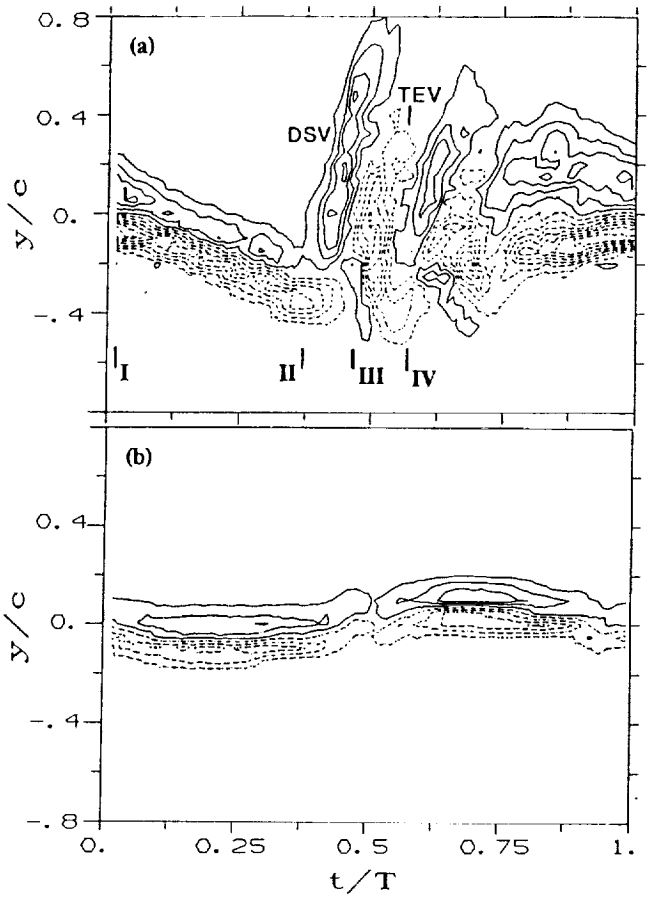

Fig. 3 Temporal distributions of $<\omega_z>c/U_\infty$; x/c = 0.3; R_c = 44,000. Contour levels start at 0.5 or -0.5 and are at interval of 0.5 (solid lines for positive and dashed lines for negative vorticity). (a) $\alpha = 15.3° + 9.7°\sin(2\pi ft-\pi/2)$, k = 0.16 (b) $\alpha = 0° + 7.2°\sin 2\pi ft$, k = 0.028.

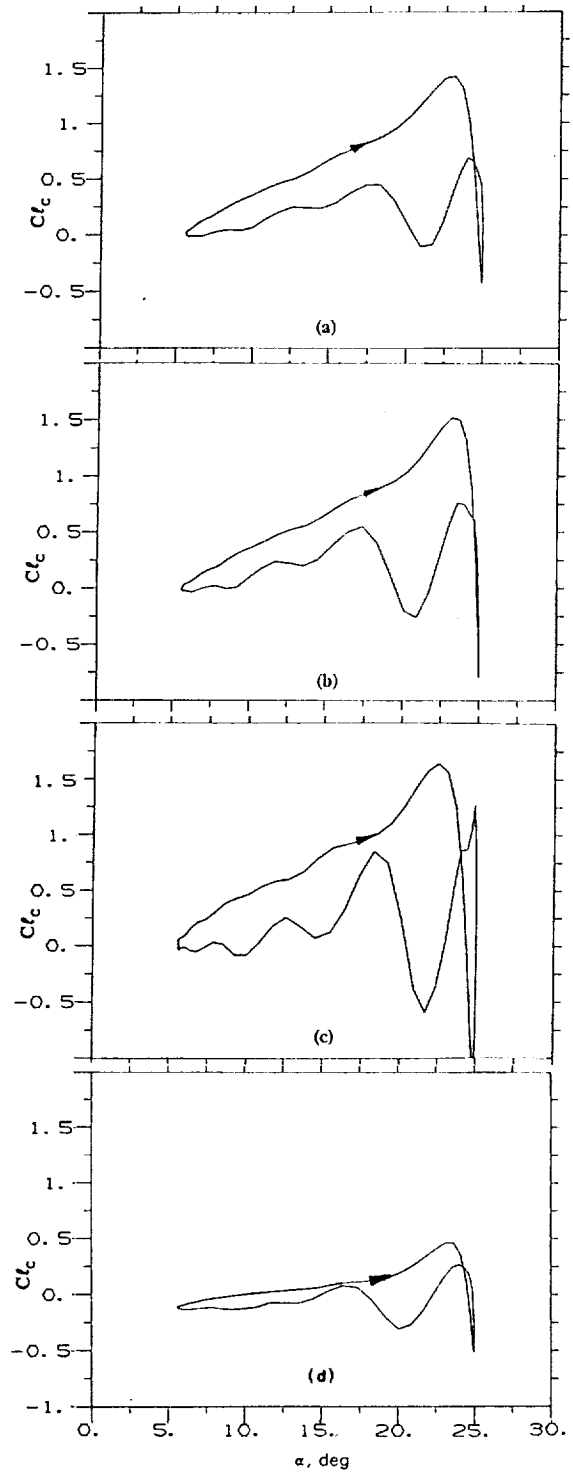

Fig. 4 Circulatory component of $C\ell$ versus α estimated from the data of Fig. 3(a); $\alpha = 15.3° + 9.7°\sin(2\pi ft-\pi/2)$, k = 0.16. (a) to (d) obtained by using Eqns. 1 to 4, respectively.

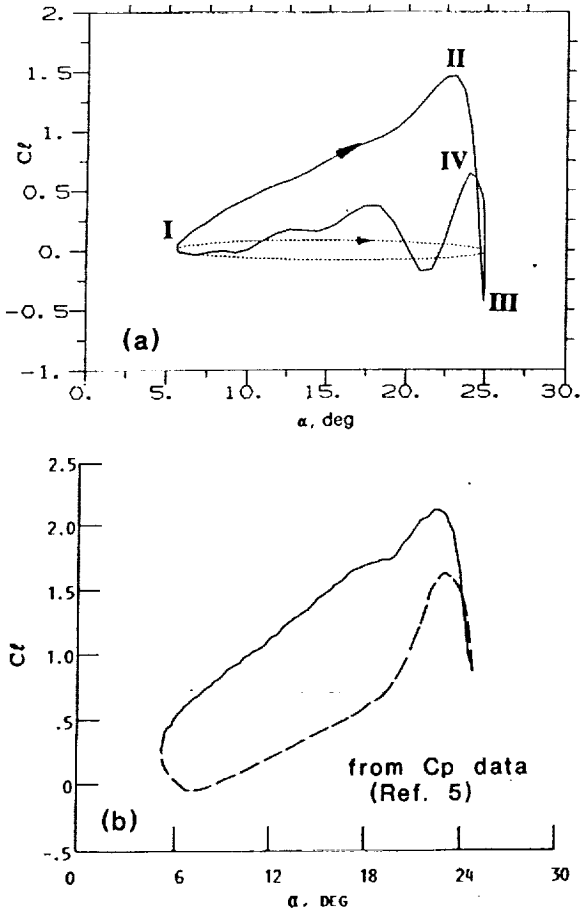

Fig. 5 $C\ell$ versus α. for oscillation at $\alpha \approx 15° + 10°\sin 2\pi ft$. (a) Unsteady component obtained by adding results of Eqn. 1 (Fig. 4a) with 'non-circulatory' component (dashed curve); k = 0.16, R_c = 44,000, M = .019. (b) Total $C\ell$ versus α; k = 0.153, R_c = 4.8 x 10^5, M = 0.036.

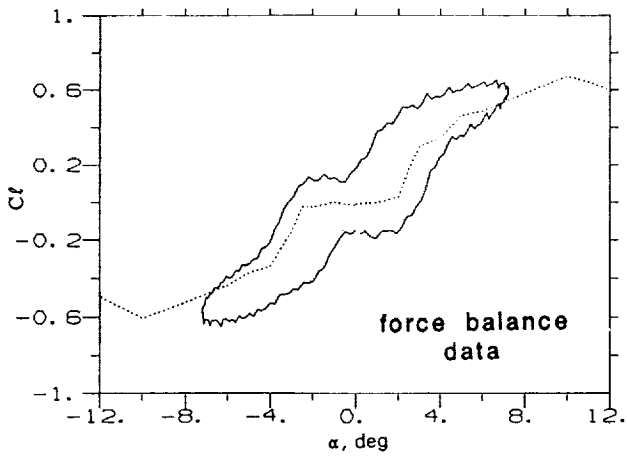

Fig. 6 Total $C\ell$ versus α for the case of Fig. 3(b): $\alpha = 0° + 7.2°\sin 2\pi ft$, k = 0.028. Dashed line for steady state variation of $C\ell$ with α.

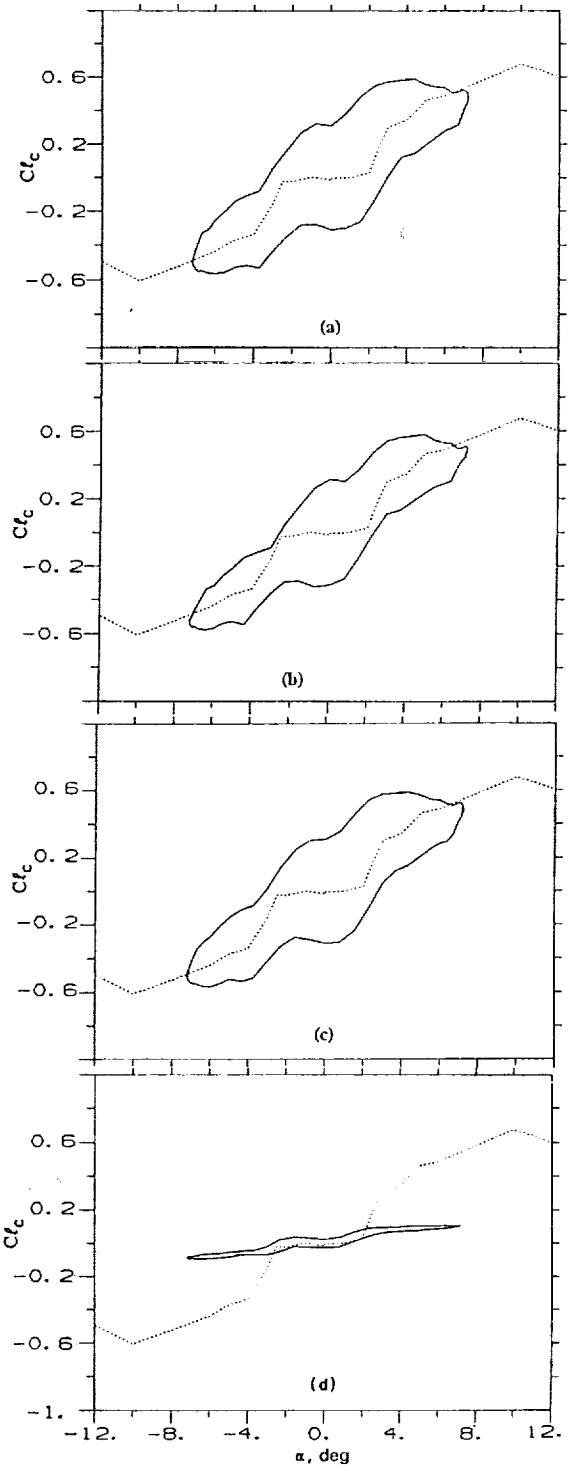

Fig. 7 Circulatory component of $C\ell$ versus α estimated from the data of Fig. 3(b); $\alpha = 0° + 7.2°\sin 2\pi ft$, k = 0.028. Figs. (a) to (d) obtained by using Eqns. 1 to 4, respectively.

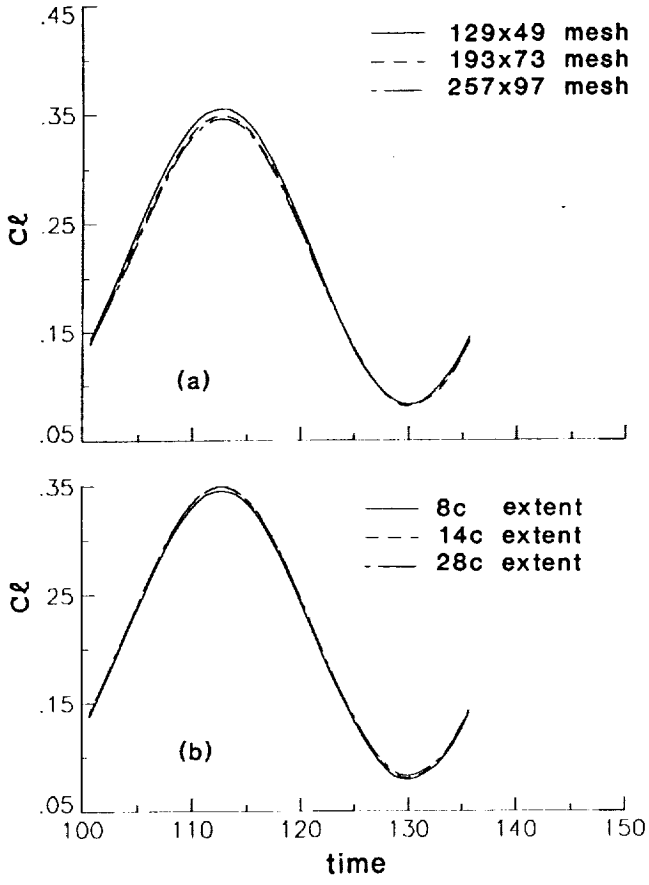

Fig. 8 Computed total Cℓ versus time obtained from Cp-distribution for $\alpha = 2° + 2°\sin 2\pi ft$; $k = 0.3$, $R_c = 44{,}000$, $M = 0.3$. Effects of: (a) grid density, (b) computational domain extent.

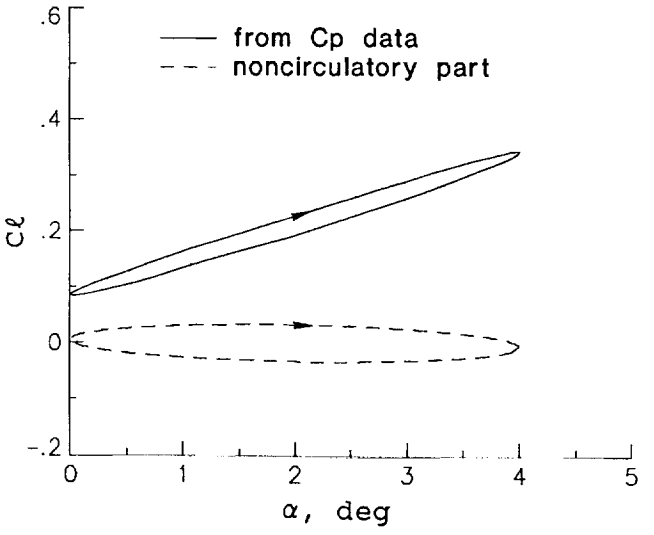

Fig. 9 Cℓ versus α corresponding to the data of Fig. 8; dashed curve for 'non-circulatory' component.

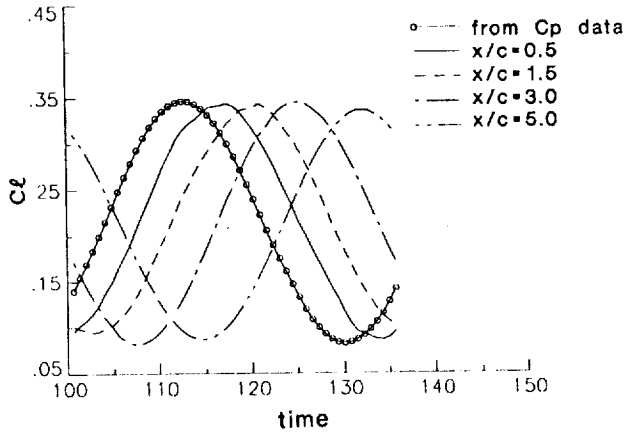

Fig. 10 Cℓ versus time obtained by Eqn. 1, from computed data at different x/c as indicated.

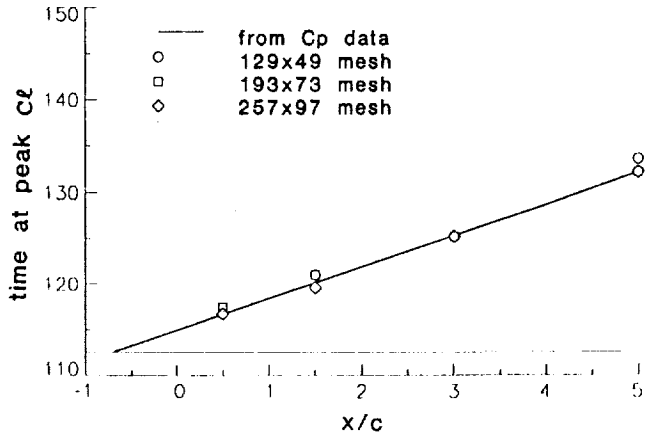

Fig. 11 Time when peak in Cℓ occurred at different x/c corresponding to the data of Fig. 10.

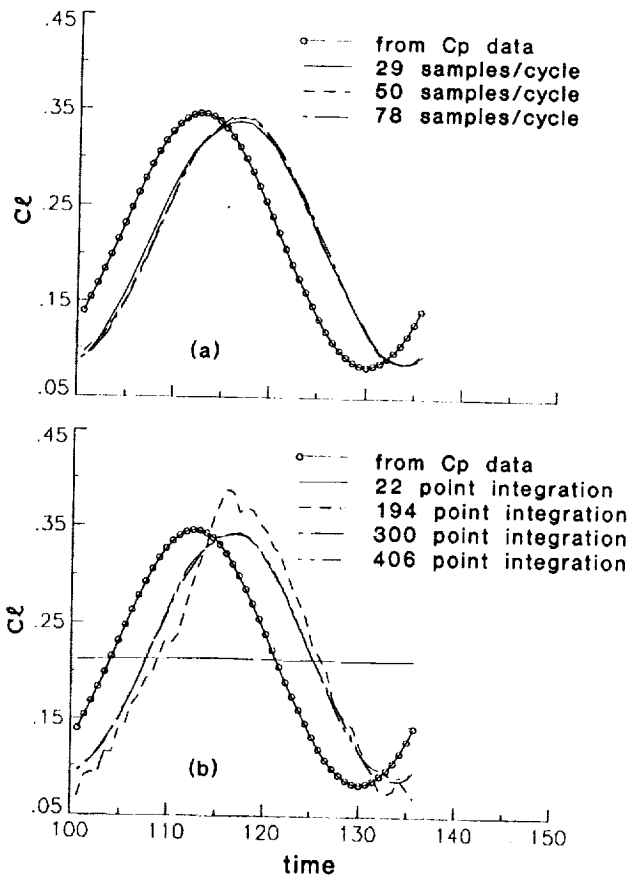

Fig. 12 Cℓ versus time obtained by Eqn. 1 from the computed data at x/c = 0.5; (a) effect of sampling rate, (b) effect of spatial resolution.

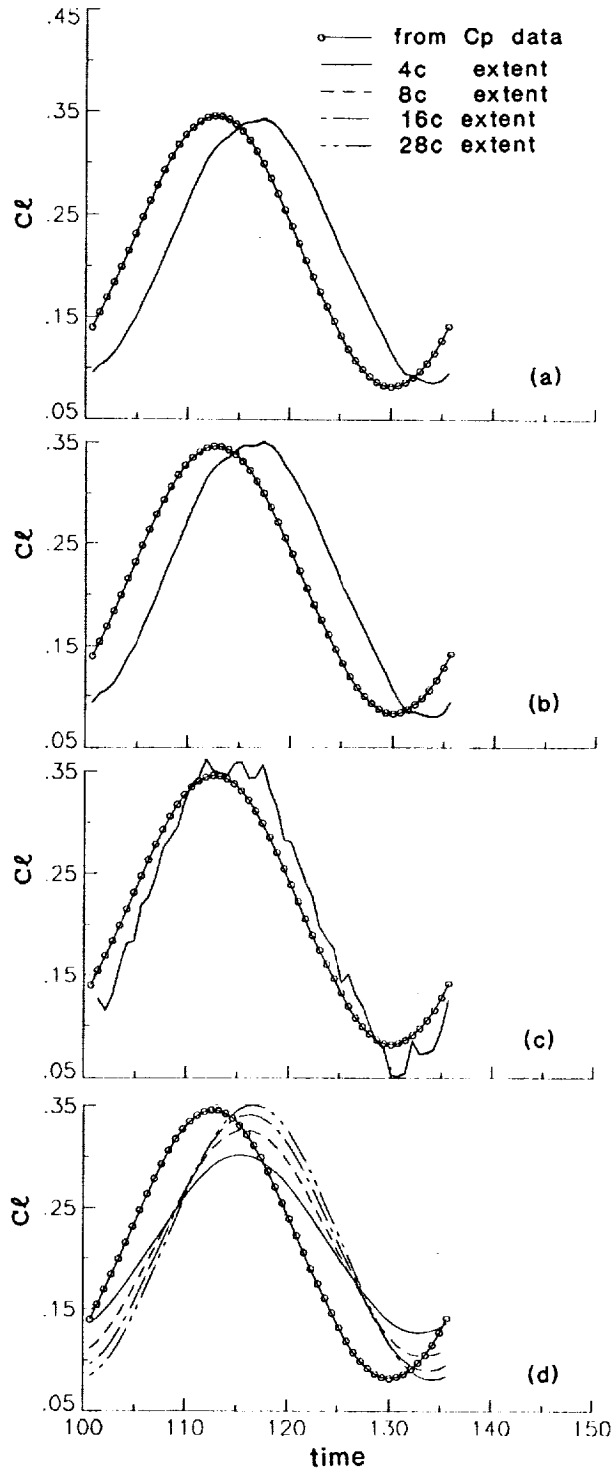

Fig. 13 Cℓ versus time obtained from computed data at x/c = 0.5. For each case, integration is performed over four transverse extents as indicated. Figs. (a) to (d) obtained by using Eqns. 1 to 4, respectively.

REPORT DOCUMENTATION PAGE

Form Approved
OMB No. 0704-0188

1. AGENCY USE ONLY (Leave blank)	2. REPORT DATE	3. REPORT TYPE AND DATES COVERED
	January 1993	Technical Memorandum

4. TITLE AND SUBTITLE
Estimation of Unsteady Lift on a Pitching Airfoil From Wake Velocity Surveys

5. FUNDING NUMBERS
WU-505-52-62

6. AUTHOR(S)
K.B.M.Q. Zaman, J. Panda, and C.L. Rumsey

7. PERFORMING ORGANIZATION NAME(S) AND ADDRESS(ES)
National Aeronautics and Space Administration
Lewis Research Center
Cleveland, Ohio 44135-3191

8. PERFORMING ORGANIZATION REPORT NUMBER
E-7465

9. SPONSORING/MONITORING AGENCY NAMES(S) AND ADDRESS(ES)
National Aeronautics and Space Administration
Washington, D.C. 20546-0001

10. SPONSORING/MONITORING AGENCY REPORT NUMBER
NASA TM-105947

11. SUPPLEMENTARY NOTES
Prepared for the 31st Aerospace Sciences Meeting and Exhibit sponsored by the American Institute of Aeronautics and Astronautics, Reno, Nevada, January 11-14, 1993.

12a. DISTRIBUTION/AVAILABILITY STATEMENT
Unclassified - Unlimited
Subject Category 02

12b. DISTRIBUTION CODE

13. ABSTRACT *(Maximum 200 words)*

The results of a joint experimental and computational study on the flowfield over a periodically pitched NACA0012 airfoil, and the resultant lift variation, are reported in this paper. The lift variation over a cycle of oscillation, and hence the lift hysteresis loop, is estimated from the velocity distribution in the wake measured or computed for successive phases of the cycle. Experimentally, the estimated lift hysteresis loops are compared with available data from the literature as well as with limited force balance measurements. Computationally, the estimated lift variations are compared with the corresponding variation obtained from the surface pressure distribution. Four analytical formulations for the lift estimation from wake surveys are considered and relative successes of the four are discussed.

14. SUBJECT TERMS	15. NUMBER OF PAGES
Dynamic stall; Unsteady separation; Lift; Wake; Airfoil	16
	16. PRICE CODE: A03

17. SECURITY CLASSIFICATION OF REPORT	18. SECURITY CLASSIFICATION OF THIS PAGE	19. SECURITY CLASSIFICATION OF ABSTRACT	20. LIMITATION OF ABSTRACT
Unclassified	Unclassified	Unclassified	